Preliminary JIRAM Results From Juno Polar Observations: 2 - Analysis of the Jupiter Southern H_3^+ emissions and Comparison with the North Aurora

A. Adriani[1], A. Mura[1], M.L. Moriconi[2], B.M. Dinelli[2], F. Fabiano[2,3], F. Altieri[1], G. Sindoni[1], S.J. Bolton[4], J.E.P. Connerney[5], S.K. Atreya[6], F. Bagenal[7], J.-C. M. C. Gérard[8], G. Filacchione[1], F. Tosi[1], A. Migliorini[1], D. Grassi[1], G. Piccioni[1], R. Noschese[1], A. Cicchetti[1], , G.R. Gladstone[4], C. Hansen[9], W.S. Kurth[10], S.M. Levin[11], B.H. Mauk[12], D.J. McComas[13], A. Olivieri[14], D. Turrini[1], S. Stefani[1] and M. Amoroso[14]

[1]INAF-Istituto di Astrofisica e Planetologia Spaziali, Roma, Italy
[2]CNR-Istituto di Scienze dell'Atmosfera e del Clima, Bologna e Roma, Italy
[3]Dipartimento di Fisica e Astronomia, Università di Bologna
[4]Southwest Research Institute, San Antonio, Texas, USA
[5]NASA Goddard Space Flight Center, Greenbelt, Maryland, USA
[6]University of Michigan, Ann Arbor, Michigan, USA
[7]University of Colorado, Boulder, Colorado, USA
[8]University of Liège, Liège, Belgium
[9]Planetary Science Institute, Tucson, Arizona, USA
[10]Jet Propulsion Laboratory, California Institute of Technology, Pasadena, California, USA
[11]University of Iowa, Iowa City, Iowa, USA
[12]The Johns Hopkins University Applied Physics Laboratory, Laurel, Maryland, USA
[13]PPPL, Princeton University, New Jersey, USA
[14]Agenzia Spaziale Italiana, Roma, Italy

Corresponding author: Alberto Adriani (alberto.adriani@iaps.inaf.it)

Key Points:

- H_3^+ intensity, column density and temperature maps of the Jupiter Southern aurora are derived from Juno/JIRAM data collected on the first orbit
- Emissions from Southern aurora are more intense than from the North.
- Derived temperatures are in the range 600 to 1400 K

Abstract

The Jupiter InfraRed Auroral Mapper (JIRAM) aboard Juno observed the Jovian South Pole aurora during the first orbit of the mission. H_3^+ (trihydrogen cation) and CH_4 (methane) emissions have been identified and measured. The observations have been carried out in nadir and slant viewing both by a L-filtered imager and a 2-5 µm spectrometer. Results from the spectral analysis of the all observations taken over the South Pole by the instrument are reported. The coverage of the southern aurora during these measurements has been partial, but sufficient to determine different regions of temperature and abundance of the H_3^+ ion from its emission lines in the 3-4 µm wavelength range. Finally, the results from the southern aurora are also compared

with those from the northern ones from the data taken during the same perijove pass and reported by *Dinelli et al.* [this issue].

1 Introduction

In Jupiter's ionosphere, H^+ and H_2^+ are produced by photoionization and electron impact ionization, with H_2^+ comprising more than 90% of the ion production rate [Atreya, 1986]. At higher altitudes, where the H density exceeds the H_2 density, charge exchange converts H_2^+ into H^+ (R1 below), which is the principal ion in the atmosphere of Jupiter. Reaction between H^+ and H_2 results in a new ion, H_3^+ (R2). In the lower altitude region, where H_2 exceeds H, reaction between H_2^+ and H_2 forms H_3^+ (R3).

$H_2^+ + H \rightarrow H^+ + H_2$ (R1)
$H^+ + 2\,H_2 \rightarrow H_3^+ + H_2$ (R2)
$H_2^+ + H_2 \rightarrow H_3^+ + H$ (R3)

H_3^+ ion converts to neutral hydrogen by dissociative recombination in the upper atmosphere and hydrocarbon ions in the lower atmosphere.
While H_3^+ has a relatively low abundance in Jupiter's ionosphere compared to the main ion, H+, its abundance can increase dramatically if H_2 is vibrationally excited [Atreya, 1986].
In the auroral region, a large magnetospheric power input of more than 10^{14} W due to precipitation of energetic charged particles can result in elevated thermospheric temperatures [e.g. Miller et al., 2006] and up to 1000 times increased H_3^+ density by the above reactions, but with H_2 now in vibrationally excited state. The detection of H_3^+ in Jupiter's atmosphere [Drossart et al., 1989] gave the first evidence of the above auroral phenomenon.
The Juno mission [Bolton et al, 2017 and Connerney et al, 2017] provides the first occasion to study the South Pole aurora of Jupiter in homogeneous and simultaneous observing conditions. Past analyses (*Kim et al.*, 2009 and 2015; *Giles et al*, 2016), conducted from ground-based observations have been challenged by using spectra obtained on different dates with different sky conditions. One of the primary objectives of the Juno mission is to clarify the auroral mechanisms at play. Its unique polar orbit provides JIRAM with many opportunities to target and detect emissions and morphology of the auroral features from different distances and from a variety of viewing angles.
JIRAM is composed by a spectrometer and an imager, sharing the same telescope [*Adriani et al*., 2014, 2016]. The imager focal plane is, in turn, divided into two equal areas defined by the superimposition of two different band-pass filters: an L-filter, centered at 3.45 μm with a 290 nm bandwidth, and an M-filter, centered at 4.78 μm with a 480 nm bandwidth. The spectrometer's slit is co-located in the M-filter imager's field of view (FOV) and its spectral range covers the 2-5 μm interval in 336 spectral bins (bands) resulting in a spectral sampling of 8.9 nm/band across the full spectral range. Each band has a spectral resolution of about 12 nm in the range 3-4 μm. The instrument design allows imaging the auroral features both spatially and spectrally in a unique session. As the spectrometer and the L-band imager (set for auroral observations) are not co-located [*Adriani et al.*, 2014], custom planning of the spectrometer measurements has been also set in the perspective to match consecutive acquisitions to obtain an almost simultaneous spatial and spectral images. The spacecraft spins perpendicular to the orbital plane in order to keep its attitude by inertia against radiation disturbances on the navigation system. JIRAM is equipped with a despinning mirror that compensates for the spacecraft rotation and enables to

keep the target image in the field of view during the data acquisition [*Adriani et al.*, 2014]. The de-spinning mirror may also be activated at different times with respect to the nadir direction, by using data about the spacecraft dynamics, allowing a scan of the planet in the spacecraft's spinning plane. No pointing outside of the spinning plane is permitted.
JIRAM spectral observations have been used in the present work to give spatially detailed analysis of H_3^+ temperatures and column densities of the South Pole aurora, assuming a quasi-local thermal equilibrium for H_3^+ [*Stallard et al*, 2002]. These results are summarized in a series of maps. In section 2 we describe the observation strategies and data management. Maps are presented along with the method applied to retrieve effective temperatures and column densities of the emitting molecules along the line of sight in Section 3. The results will also be discussed and compared with the findings reported in the previous literature. Other specific auroral topics such as morphology and dynamics are described by *Mura et al.* (this issue).

2 Observations and Data Management

The first JIRAM observations of the Southern aurora were acquired on 27 August 2016, in the outbound leg of the first orbit, from 15:00 to 19:45 UTC. During that period, the spacecraft was moving away from the planet and the instrument had the Jupiter's southern hemisphere in its field of view. The spatial resolution at the 1-bar level ranged between 45 and 135 km. The spectrometer's slits mosaic reported in Figure 1 gives the complete survey of the spectral observations of the Southern aurora. The spectral mosaic is superimposed to a single L-band image taken by the JIRAM imager for context reference. Figure 1 has been mapped in a polar stereographic projection. The acquisitions have been jovian-located and then re-projected in Sys III planetocentric geographical coordinates. Geometric information was obtained by using ad hoc algorithms based on the NAIF-SPICE tool [*Acton*, 1996] for each image of the spectrometer and imager channels. JIRAM raw data are radiometrically calibrated in units of spectral radiance (W/m^2 μm sr) as described by *Adriani et al.* [2014]. It should be noted that the L-band side of the imager and the spectrometer's slit do not simultaneously observe the same scene, even though they are operated at the same time. Indeed, the spectrometer slit is optically combined with the M-band side of the imager dedicated to the thermal emission of the planet. The L-band imager covers a FOV of about 1.75° by 6° while the spectrometer's slit is sampled in 256 spatial pixels, each with an individual field of view (IFOV) of about 240 μrad for a total coverage of about 3.5° (see *Adriani et al.*, 2104, for instrumental details). Imager and spectrometer pixels have the same individual IFOV. However the spectrometer slit can scan the same area of the L-band imager in times subsequent to the imager acquisition. Figure 1 is a RGB color composition of the southern aurora observed during the first pass at the perijove (PJ1), where the mosaic from the imager has been set in red while the green and the blue correspond to two different spectrometer channels selected among the H_3^+ emission line wavelengths. The green one corresponds to the 3.315 μm wavelength, where the H_3^+ emission is superimposed to the CH_4 Q branch, and indicates wherever this hydrocarbon is present and emitting. The blue one is set at 3.54 μm, where the infrared aurora has one of its stronger emission bands. This rendering emphasizes the coincidence of the main oval features between spectrometer and imager. Indeed the auroral structure appears white where the two images overlap, attesting that the green and blue spectral traces spatially converge on the red imager one. The size of the pixels on the figure is proportional to the actual spatial dimension of the instrument pixels. The transition of the image color from white to green in the inner part of auroral oval suggests a non-negligible presence of methane being the 3.315 μm band amplitude significantly higher than expected for H_3^+ compared to the other emission bands.

3 Analysis and Discussion

Figure 2 reports the observational parameters for the southern hemisphere where the spectrometer data are available. According to the models by *Grodent et al.* [2001] and *Uno et Al.* [2014] the 500-km surface is expected to be closer to the real position of the maximum of the excited H_3^+. Therefore, in order to provide a more accurate match of the auroral features with respect to the underlying planet for slant observations, each spatial pixel is plotted on a stereographic map referred to a surface at 500 km above the 1-bar reference level. The radiances corresponding to the H_3^+ emission band between 3.35 and 3.75 μm have been integrated to highlight the position of the H_3^+ aurora and avoid spectral contamination from methane at 3.315 μm. The integrated radiances have been multiplied by the cosine of the emission angle, to correct for the observational slant optical path. The dashed curve gives the position of the UV statistical auroral oval based on HST observations of the southern aurora [*Grodent et al.*, 2003]. The continuous curve indicates the predicted position by the VIP4 model [*Connerney et al.*, 1998]. During the period of acquisition the planet rotated about 180° so that we cannot address any specific direction related to the Sun in the maps. Beside the integrated radiance, Figure 2 also gives additional information about the observations, such as the Jupiter time of the day related to the solar position with respect to the observational attitude, the solar zenith angle (SZA) and the emission angle. All the observations of the southern aurora have been made on the Jovian dayside and no measurements are available for the night side during PJ1. The absolute and relative intensities of the H_3^+ emission bands are directly related respectively to the number of emitting ions and their effective temperatures, so the H_3^+ column densities and temperatures have been computed using the method described by *Dinelli et al.* [this issue] and applied to the analysis the northern hemisphere auroral data. According to this method the intensity of each transition k of any molecule M can be computed using the expression reported by *Altieri et al.* [2016] taken from *Stallard et al.* [2002, and references therein]. In the retrieval analysis the presence of methane, as an additional contributor to the spectral signatures, had to be taken into account to avoid contaminating the auroral information coming from the H_3^+ ion. H_3^+ effective temperatures and column densities have been obtained only for the measurements where the infrared auroral emissions are present. Only spectra with an emission angle smaller than 75° have been retained in the analysis and the results of the analysis were further filtered by retaining the retrievals for which the final χ^2 test was smaller than 20 and the obtained temperatures had a random error (the error due to the mapping of the measurement noise onto the retrieved parameters) lower than 100 K [*Dinelli et al.*, this issue]. No filter was applied to the size of the error on the H_3^+ column densities. As an example, Figure 3 shows a typical spectrum collected in correspondence of oval where the H_3^+ emission bands (black curve) appear to be not contaminated by the methane emission. A H_3^+ spectrum contaminated by the presence of the CH_4 Q-band emission at 3.315 μm is also shown in red in the same picture. That spectrum has been acquired in a region inside the oval and closer to South Pole. In the same figure the dashed curves show the respective modeled spectra used to determine the H_3^+ temperature and the column density. More details on the analysis and the relative discussion about the presence of methane auroral emissions are matter of a separate paper by Moriconi et al. [this issue].

Figure 4 shows the H_3^+ temperature field, whose values range between 850K and 1100K. The orthographic projections of the data shown in the different panels of Figure 4 have been divided into squared bins, obtained by dividing each axis in regular intervals. Then, the individual parameters to map have been averaged over each bin and bins containing less than 3 measurements have been discarded. Figures 4 represents the contour plots of the binned distributions. In general, the temperature field of the aurora looks quite patchy with a tendency to decrease inside the oval. The error on the retrieved temperatures is always below 10% but the presence of methane in the auroral scene impacts the H_3^+ temperature retrieval to some extent. Even if the methane emission was included in the retrieval, the largest values of the error are obtained where the methane emissions prevails because in those areas the H_3^+ signal is very weak (see Figure 1). The highest temperature along the oval can be found on the morning side as it can be seen by comparing the temperature maps in Figure 4 and the local solar time during the observations in Figure 2 where it reaches values as high as 1100K. The H_3^+ column density is also mapped in Figure 4. The values range in the interval 1-3.5x10^{12} ions/cm^{-2}. After the retrieval the H_3^+ column has been corrected by the emission angle so that values in Figure 4 represent the equivalent vertical column of emitting H_3^+ ions. Therefore the distribution of the integrated radiance shown in Figure 2 follows the distribution of the column density reported in Figure 4. The relative error on the retrieved values is less than 10% and the highest error values are in correspondence of the methane presence where H_3^+ presents the lowest column densities.
As previously mentioned the observations of the southern aurora were collected during daytime only while the northern observations cover the full Jupiter day of about 10 hours. A comparison between the southern and northern auroral emissions [see *Dinelli et al.*, this issue] is given in Figure 5 and the comparison is shown for the period of the day in which both southern and northern data are both available, namely from about 3 to 7 hours (time of the Jovian day). Figure 5 shows different panels that account for various auroral parameters like the 3.35-3.75 μm integrated radiance and H_3^+ effective temperature as a function of the solar time on the left column. The curves have been obtained as running averages on the single parameter values for a number of points corresponding to about a 1 h time interval. The right column, instead, reports correlations between the same retrieved parameters. A North/South direct comparison shows that the integrated radiances display systematic differences. Southern hemisphere auroral emissions appear generally to be always stronger than the northern ones. In the southern hemisphere the average integrated radiance was (0.89±0.46)x10^{-4} W m^{-2} sr^{-1} with values reaching 7.34x10^{-4} W m^{-2} sr^{-1} while in the North no values greater than 3.38x10^{-4} W m^{-2} sr^{-1} have been found with a mean value of (0.75±0.34)x10^{-4} Wm^{-2}sr^{-1} (see also Figure 5) [*Dinelli et al.*, this issue]. As expected, integrated radiances are proportional to the column densities but temperatures show a different behavior: namely temperatures tend to be higher for lower column densities. A limited number of auroral regions reach temperatures as high as 1400K in correspondence with column densities of about 0.5x10^{12} ions/cm^2. By contrast, the largest column densities values (namely above 4.0x10^{12} ions/cm^2) correspond to temperatures mostly around 900K. By using data from the first Jupiter flyby, the comparison between South and North is not straightforward with respect to their trends versus the time of the day. If we consider the period of the day when South and North may be compared, the number of observations from the North is more limited and not widely distributed over space. The Northern auroral observations taken during the central part of the day mostly originate from regions inside the oval (see *Dinelli et al.*, this issue) so that the low values of radiances and temperatures have to be mostly attributed to the location of the auroral emissions. Instead, observations taken in the first part of the morning and in the afternoon come

from the oval regions. Differently from the North, greater information about the diurnal trend of the emissions intensity can be found in the Southern data that shows an increase at dawn and before dusk. In order to verify this behavior three independent longitudinal intervals have been selected. Those longitudinal intervals have been observed at different times of the day (see the lower left panel of Figure 5). All three areas show the same behavior of the emissions during the day, namely a decrease of the emission during the central part of the day and higher values closer to dawn and dusk. In general, the highest temperatures in the southern hemisphere appear to be reached in the first part of the morning, while staying approximately constant during the rest of the day. *Majeed et al.* [2009] used a thermosphere/ionosphere model to quantify thermal processes that take place in the auroral thermosphere and our observations confirm their results. Moreover, *Cohen and Clarke* [2011] also modeled the South-North differences in the auroral temperatures referring to the temperature profile of Grodent et al. [2001] obtained on the basis of the observations of the UV aurora made with the Hubble Space Telescope. However, the present observations do not permit to discriminate the variation of the H_3^+ emission versus the altitude but they account for the emissions originating from the full H_3^+ columns. Nevertheless the observed North-South temperature difference agrees with the prediction of the models. In fact, it results that both emissions and temperatures retrieved from the Southern aurora are, in the average, always significantly higher than the ones observed in the North. The reason for these differences is not well understood but it could be linked to the combination of the asymmetry in the location of the magnetic poles respect the planet rotation axis and the circulation of hydrogen in the upper atmosphere.

4 Concluding Remarks

The spatial distribution of temperatures and column densities of the H_3^+ ions responsible for the southern auroral emissions have been analyzed in detail for the first time based from Juno/JIRAM data. In some of our maps, the auroral shape has also been compared with the auroral spatial position predicted by the VIP4 model of *Connerney et al.*, [1998]. The observed auroral oval is also shown in comparison with its average spatial position computed on the basis of many years of ground-based observations and according to the statistical model reported in *Grodent et al.* [2003]. As a result, the auroral oval seems to be in better agreement with the statistical model rather than with the VIP4 one. The retrieved temperatures can vary between 600K and 1400K during the Jovian day with prevalence of higher values in the morning and the column densities range between 0.2 and $4.0\text{x}10^{12}$ ions/cm^2. A comparison of the southern auroral with the northern auroral regions shows significant differences with the northern aurora both in magnitude and behavior.

Acknowledgments

The JIRAM project is founded by the Italian Space Agency (ASI). In particular this work has been developed under the agreement n. 2016-23-H.0. JCG acknowledges support from the PRODEX program of the European Space Agency in collaboration with the Belgian Science Policy Office.

The data will be available once the proprietary period ends at https://pds.jpl.nasa.gov/tools/data-search/

References

Acton, C.H., (1996). Ancillary data services of NASA's navigation and ancillary information facility. Planet. Space. Sci. 44 (1), 65-70

Adriani A., G. Filacchione, T. Di Iorio, D. Turrini, R. Noschese, A. Cicchetti, D. Grassi, A. Mura, G. Sindoni, M. Zambelli, G. Piccioni, M.T. Capria, F. Tosi, R. Orosei, B.M. Dinelli, M.L. Moriconi, E. Roncon, J.I. Lunine, H.N. Becker, A. Bini, A. Barbis, L. Calamai, C. Pasqui, S. Nencioni, M. Rossi, M. Lastri, R. Formaro, A. Olivieri (2014), JIRAM, the Jovian Infrared Auroral Mapper. Space Sci. Rev., DOI 10.1007/s11214-014-0094-y.

Adriani A., M.L. Moriconi, A. Mura, F.Tosi, G. Sindoni, R. Noschese, A. Cicchetti, G. Filacchione, (2016), Juno's Earth flyby: the Jovian infrared Auroral Mapper preliminary results, Astrophys Space Sci, DOI 10.1007/s10509-016-2842-9

Altieri, F., B. M. Dinelli, A. Migliorini, M. L. Moriconi, G. Sindoni, A. Adriani, A. Mura, and F. Fabiano (2016), Mapping of hydrocarbons and H_3^+ emissions at Jupiter's north pole using Galileo/NIMS data Geophys. Res. Lett. , 43, 11,558{367 11,566, doi:10.1002/2016GL070787.

Atreya, S. K. (1986). Atmospheres and Ionospheres of the Outer Planets and their Satellites, pp 106-144, Springer-Verlag, New York-Berlin-Heidelberg.

Bolton S.J., A. Adriani, V. Adumitroaie, J. Anderson, S. Atreya, J. Bloxham, S. Brown, J. E.P. Connerney, E. DeJong, W. Folkner, D. Gautier, S. Gulkis, T. Guillot, C. Hansen,W.B. Hubbard, L. Iess, A. Ingersoll, M. Janssen, J. Jorgensen, Y. Kaspi, S. M. Levin, C. Li, J. Lunine, Y. Miguel, G. Orton, T. Owen, M. Ravine, E. Smith, P. Steffes, E. Stone, D. Stevenson, R. Thorne, J. Waite, (2017), in print on Science

Cohen I.J. and J.T. Clarke (2011) Modeling of Jupiter's auroral curtain and upper atmospheric thermal structure, Journal Of Geophysical Research, Vol. 116, A08205, doi: 10.1029/2010JA016037.

Connerney, J. E. P., M. H. Acuña, N. F. Ness, and T. Satoh (1998) New models of Jupiter's magnetic field constrained by the Io flux tube footprint, J. Geophys. Res., 103(A6), 11,929–11,939.

Connerney J. E.P., A. Adriani, F. Bagenal, J. Bloxham, S. J. Bolton, S. Cowley, J-C. Gerard, G.R. Gladstone, D. Grodent, G. Hospodarsky, J. Jorgensen, W. Kurth, S. M. Levin, B. Mauk, D. McComas, A. Mura, C. Paranicas, (2017), in print on Science

Dinelli B.M., F. Fabiano, A. Adriani, F. Altieri, M.L. Moriconi, A. Mura, G. Sindoni, G. Filacchione, F. Tosi, A. Migliorini, D. Grassi, G. Piccioni, R. Noschese, A. Cicchetti, S.J. Bolton, J.E.P. Connerney, S.K. Atreya, F. Bagenal, G.R. Gladstone, C. Hansen, W.S.

Kurth, S.M. Levin10 , B.H. Mauk, D.J. McComas, J.-C. Gerard, D. Turrini, S. Stefani, M. Amoroso, and A. Olivieri (2017) Preliminary JIRAM Results from Juno Polar Observations: 1 - Methodology and Analysis Applied to the Jovian Northern Polar Region, this issue.

Drossart, P. et al. (1989). Detection of H3+ on Jupiter, Nature, 340, 539

Giles R.S., L.N. Fletcher, P.G.J. Irwin, H. Melin, and T.S. Stallard (2016), Detection of H_3^+ auroral emission in Jupiter's 5-micron window, A&A 589, A67 (2016), DOI: 10.1051/0004-6361/201628170

Grodent, D., J.H. Waite Jr., and J.C. Gerard (2001),A self-consistent model of the Jovian auroral thermal structure, J. Geophys. Res., 106(A7), 12,933–12,952, doi:10.1029/2000JA900129.

Grodent D., J.T. Clarke, J. Kim, J.H. Waite Jr., and S.W.H. Cowley (2003), Jupiter's main auroral oval observed with HST-STIS, Journal Of Geophysical Research, Vol. 108, No. A11, 1389, doi:10.1029/2003JA009921.

Kim, S. J., C.K. Sim, J. Ho, T.R. Geballe , Y.L. Yung, S. Miller, Y.H. Kim (2015). Hot CH4 in the polar regions of Jupiter, Icarus, 257, 217–220.

Kim, S. J, T.R. Geballe , H.J. Seo, Y.H. Kim, (2009). Jupiters's hydrocarbon polar brightening: Discovery of 3-micron line emission from south polar CH4, C2H2, and C2H6, Icarus, 202, 354–357.

Majeed, T., J. H. Waite, S. W. Bougher, and G. R. Gladstone (2009), Processes of auroral thermal structure at Jupiter: Analysis of multispectral temperature observations with the Jupiter Thermosphere General Circulation Model, J. Geophys. Res., 114, E07005, doi:10.1029/2008JE003194.

Miller, S. et al. (2006). H3+: the driver of giant planet atmospheres, Phil. Trans. R. Soc. A (2006) 364, 3121–3137, doi:10.1098/rsta.2006.1877.

Moriconi M.L., A. Adriani, B.M. Dinelli, F. Fabiano, F. Altieri, F. Tosi, G. Filacchione, A. Migliorini, A. Mura, D. Grassi, G. Sindoni, G. Piccioni, R. Noschese, A. Cicchetti, S.J. Bolton, J.E.P. Connerney, J. C. Gérard, S.K. Atreya, F. Bagenal, G.R. Gladstone, C. Hansen, W.S. Kurth, S.M. Levin, B.H. Mauk, D.J. McComas, D. Turrini, S. Stefani, A. Olivieri, and M. Amoroso (2017), Preliminary JIRAM Results from Juno Polar Observations: 3 –Evidence of Diffuse Methane Presence in the Jupiter Auroral Regions, this issue.

Mura A., A. Adriani, F. Altieri, J.E.P. Connerney, S.J. Bolton, M.L. Moriconi, J-C. Gérard, W.S. Kurth, B.M. Dinelli, F. Fabiano, F. Tosi, S.K. Atreya, F. Bagenal, G.R. Gladstone, C. Hansen, S.M. Levin, B.H. Mauk, D.J. McComas, G. Sindoni, G. Filacchione, A. Migliorini, D. Grassi, G. Piccioni, R. Noschese, A. Cicchetti, D. Turrini, S. Stefani, M. Amoroso and A. Olivieri (2017), Infrared observations of Jovian aurora from Juno's first orbits: main oval and satellite footprints, this issue.

Stallard T., S. Miller, G. Millward, R.D. Joseph, 2002. On the Dynamics of the Jovian Ionosphere and Thermosphere. II The Measurement of H_3^+ Vibrational Temperature, Column Density, and Total Emission, Icarus, 156, 498–514.

Uno, T., Y. Kasaba, C. Tao, T. Sakanoi, M. Kagitani, S. Fujisawa, H. Kita, and S. V. Badman (2014), Vertical emissivity profiles of Jupiter's northern H3+ and H2infrared auroras observed by Subaru/IRCS, J. Geophys. Res. Space Physics, 119, 10,219–10,241, doi:10.1002/2014JA020454.

Figure captions

Figure 1. RGB spectrometer-imager composition of the southern aurora. The Red channel comes from an imager acquisition of the aurora (4.54-5.02 µm). Green is set at 3.31 µm where the H_3^+ emission is overlaid to the CH_4 Q branch, and blue is set at 3.54 µm, a H_3^+ emission band. The green and blue channels are composed from the spectrometer's data. The spectral data do not completely cover the imager acquisition. Colors would be affected by both brightness and relative amplitude of the RGB bands. Black corresponds to the absence of data.

Figure 2. Southern aurora observational parameters: H_3^+ auroral emissions integrated in the range 3.35 to 3.75 µm (upper left); Time of the Jovian day, namely local time for each observation point (upper right); Solar Zenith Angle (SZA) (lower left); and Emission Zenith Angle (angular direction of the spacecraft in respect the emitting area) (lower right). The single pixels of the spectrometer slit are reported with a different color according to the value of the represented parameter in each map. Latitudes are spaced by 10 degrees. The continuous curve oval shows the auroral location according to the VIP4 model [*Connerney et al.*, 1998]; the dashed curve oval is the UV statistical aurora from Hubble images [*Grodent et al.*, 2003].

Figure 3. Spectra collected in the area of the auroral oval (black curve) and in the inner part of the oval (red curve). The dashed curves are the corresponding modeled spectra obtained by the retrieval method from *Dinelli et al.* [this issue] and used for computing H_3^+ temperatures and column densities. The error on the observed values (not shown) is 1.5×10^{-4} $Wm^{-2}\mu m^{-1}sr^{-1}$.

Figure 4. Upper panels: H_3^+ effective temperature (left panel) and error on its retrieval (right panel). Lower panels: H_3^+ column density (left panel) and error on its retrieval (right panel**).** The continuous oval curve is from VIP4 model [*Connerney et al.*, 1998]; the dashed curve is the UV statistical oval reported by *Grodent et al*., [2003]. Latitude lines are spaced by 10 degrees. The orthographic projection that contains the 60° latitude South circle is divided into 50 x 50 bins for each map. Then, all the measurement points falling in each single bin are averaged to produce the contour plots shown in the figure.

Figure 5. Upper left panel: local time dependence of the H_3^+ integrated radiance (emissions in the range 3.35 and 3.75 µm) versus the Jovian time of the day; central left panel: H_3^+ effective

temperature versus the Jovian time of the day, the colored regions account for the respective retrieval errors on the temperature; lower left panel: trends of the integrated radiances during the jovian day in three different longitudinal sectors of the southern aurora. The error on the integrated radiances reported in the panels is less than $0.7x10^{-5}$ $Wm^{-2}sr^{-1}$. Scatter plots between temperature and integrated radiance (upper right), temperature and column density (central right), and column density and integrated radiance (lower right). In the scatter plots the northern auroral data are shown in blue and southern ones are in red.

Figure 1.

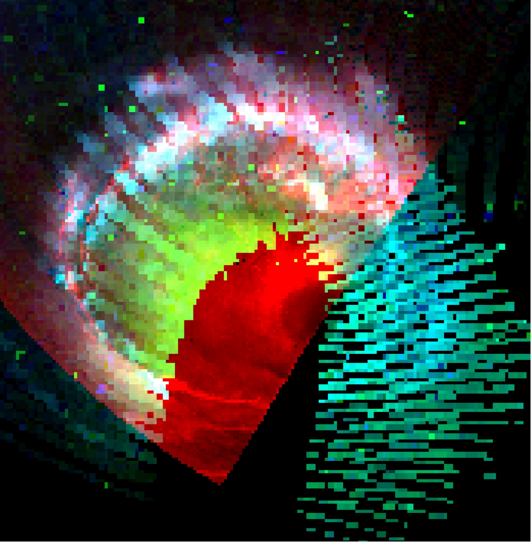

Figure 2.

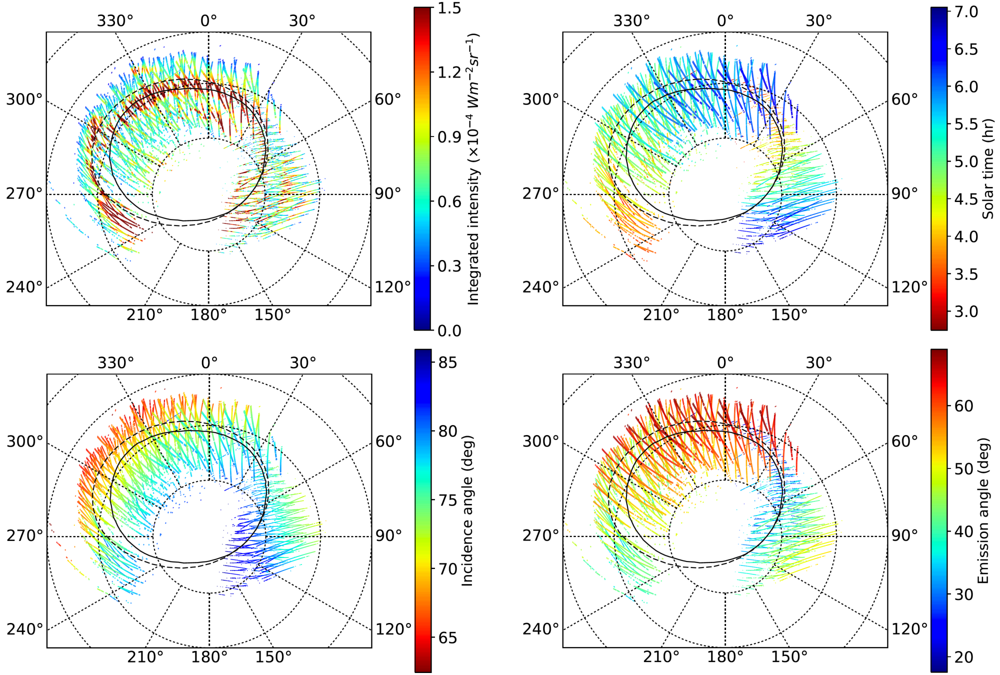

330°
0°
30°
300°
60°
270°
90°
240°
120°
210°
180°
150°
Integrated intensity ($\times 10^{-4}$ $Wm^{-2}sr^{-1}$)
0.0
0.3
0.6
0.9
1.2
1.5
Solar time (hr)
3.0
3.5
4.0
4.5
5.0
5.5
6.0
6.5
7.0
Incidence angle (deg)
65
70
75
80
85
Emission angle (deg)
20
30
40
50
60

Figure 3.

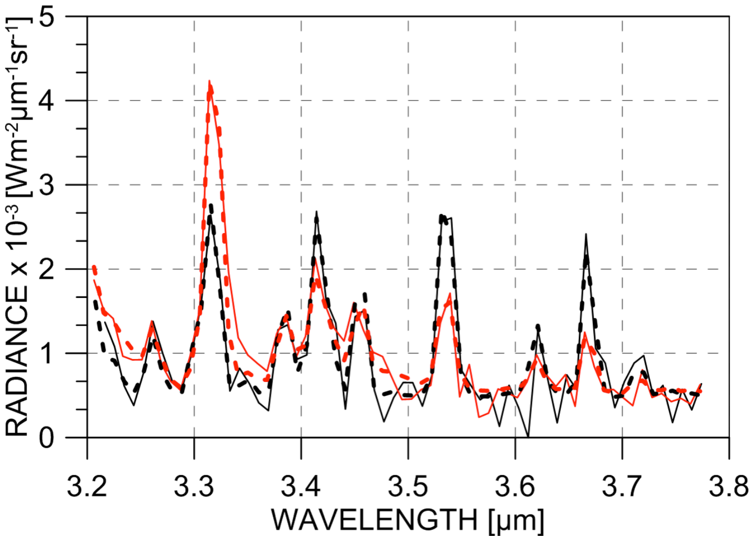

RADIANCE x 10-3 [Wm-2μm-1sr-1]
0
1
2
3
4
5
3.2
3.3
3.4
3.5
3.6
3.7
3.8
WAVELENGTH [μm]

Figure 4.

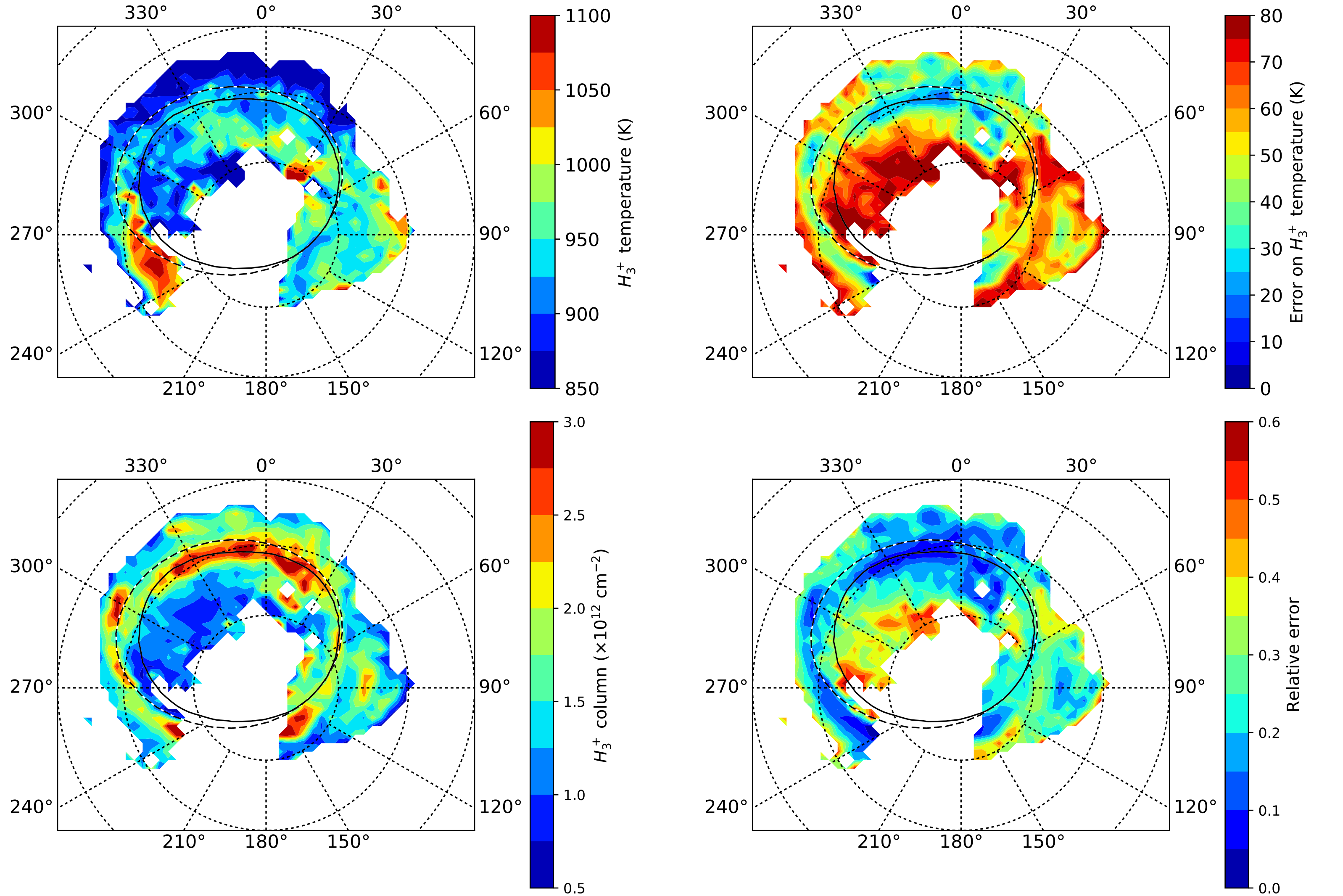

330°
0°
30°
300°
60°
270°
90°
240°
120°
210°
180°
150°
1100
1050
1000
950
900
850
H_3^+ temperature (K)
80
70
60
50
40
30
20
10
0
Error on H_3^+ temperature (K)
3.0
2.5
2.0
1.5
1.0
0.5
H_3^+ column ($\times 10^{12}$ cm^{-2})
0.6
0.5
0.4
0.3
0.2
0.1
0.0
Relative error

Figure 5.

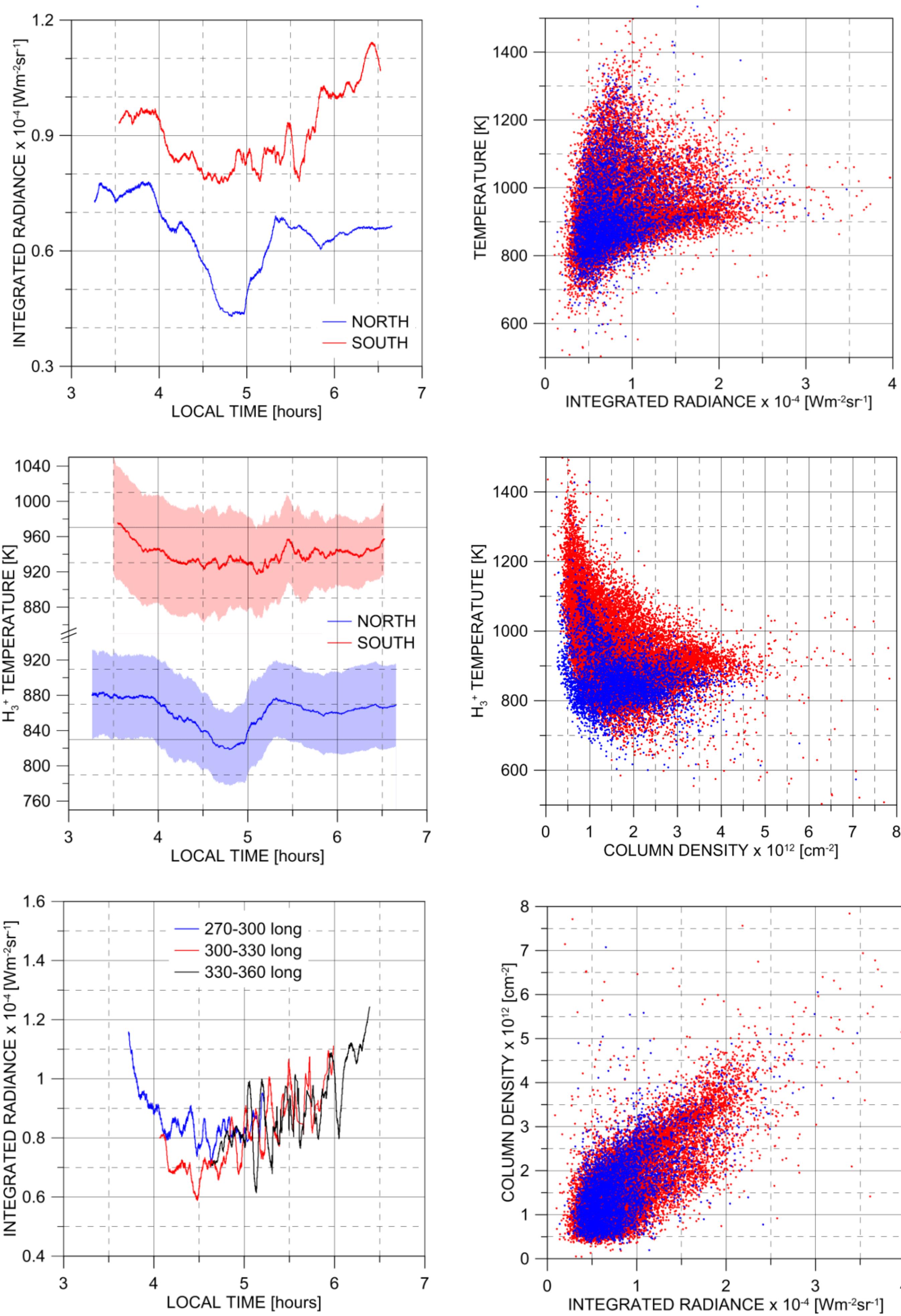

INTEGRATED RADIANCE x 10-4 [Wm-2sr-1]
LOCAL TIME [hours]
NORTH
SOUTH
TEMPERATURE [K]
INTEGRATED RADIANCE x 10-4 [Wm-2sr-1]
H3+ TEMPERATURE [K]
LOCAL TIME [hours]
NORTH
SOUTH
H3+ TEMPERATUTE [K]
COLUMN DENSITY x 1012 [cm-2]
INTEGRATED RADIANCE x 10-4 [Wm-2sr-1]
LOCAL TIME [hours]
270-300 long
300-330 long
330-360 long
COLUMN DENSITY x 1012 [cm-2]
INTEGRATED RADIANCE x 10-4 [Wm-2sr-1]